Interfacial microrheology as a tool to study viscoelastic transitions in nanoconfined soft matter

A. K. Kandar, R. Bhattacharya, and J. K. Basu
Department of Physics, Indian Institute of Science, Bangalore 560 012, India
(Received 21 November 2009; revised manuscript received 25 March 2010; published 15 April 2010)

We present a method to perform *in situ* microrheological measurements on monolayers of soft materials undergoing viscoelastic transitions under compression. Using the combination of a Langmuir trough mounted on the inverted microscope stage of a laser scanning confocal microscope we track the motion of individual fluorescent quantum dots partly dispersed in monolayers spread at the air-water interface. From the calculated mean square displacement of the probe particles and extending a well established scheme of the generalized Stokes-Einstein relation in bulk to the interface we arrive at the viscoelastic modulus for the respective monolayers as a function of surface density. Measurements on monolayers of glassy as well as nonglassy polymers and a standard fatty acid clearly show sensitivity of our technique to subtle variations, in the viscoelastic properties of the highly confined materials under compression. Evidence for possible spatial variations of such viscoelastic properties at a given surface density for the fatty acid monolayer is also provided.

DOI: 10.1103/PhysRevE.81.041504 PACS number(s): 68.47.Pe, 46.35.+z, 47.57.Qk, 68.03.−g

I. INTRODUCTION

Soft materials in general and complex fluids in particular when confined to dimensions comparable to their intrinsic structural and dynamical length scales tend to show deviation in mechanical and dynamical and related properties as compared to those observed in their respective bulk form [1–8]. Various indirect methods have been used to infer changes in properties of soft materials confined at interface, such as the glass transition temperature (T_g) or melting/solidification temperatures etc. [1–8]. However, lack of direct measurements with controlled variation of degree of confinement and the properties of the confining interfaces have lead to controversy and ambiguity regarding the nature of changes that confined complex fluids, supposedly, undergo in confinement. Confining materials at fluid-fluid interfaces using the Langmuir-Blodgett (LB) technique is an ideal method to study properties of quasi-two-dimensional (2D) systems in a controlled way by variation not only of parameters like surface density, Γ and, but also properties and parameters of the confining fluid phases [9–17], such as temperature, T. However, performing *in situ* measurements of rheological or mechanical properties, of such complex confined fluids, using the LB technique is quite challenging due to the difficulty of accessing the fluid-fluid interface for such measurements. Recently, interface rheology measurements at the fluid-fluid interface has been demonstrated by the groups of Fuller using an interfacial stress rheometer (ISR) [18] and by the group of Sood using a modification of a conventional rheometer [19] to perform measurements at interface. However the measurements performed by the latter on various monolayers cannot be performed with any degree of control over morphology or areal density as can be achieved with a Langmuir trough and the sensitivity of the measurements to interface properties cannot be easily quantified. The ISR, on the other hand, is based on Langmuir trough and hence the interface rheology measurements can be done with greater control over the monolayer conditions. However, one of the limitations of the technique is the frequency range, which can be probed which is currently available from 0.1–10 Hz [18]. More over, the size (~250 μm) and inertia of the typical probes used is a limitation on the surface sensitivity of the technique [20]. In addition no information on possible spatial variation of rheological properties of structurally heterogeneous materials can be obtained.

However, both the techniques have been used to study surface rheological phase transitions in soft matter systems. Dynamics in soft and granular materials, especially around viscoelastic transitions such as glass formation and sol-gel transition has been experimentally studied in bulk using mostly rheology based techniques [21–24]. Numerical simulations and theoretical calculations have shown the complex nature of the spatiotemporal behavior of dynamics in such systems which conventional bulk rheological measurements are unable to observe directly [25–27]. Bulk microrheological (MR) measurements based on particle tracking methods [20,28] have provided direct visualization of the spatiotemporal heterogeneity of dynamics in such systems around the glass or jamming transitions [21,22,29,30]. In addition bulk MR based techniques have also provided valuable insight into dynamics of microscopic probe particles in structurally inhomogeneous viscoelastic fluids and their micromechanical properties [31–34]. It is clear that establishment of an equivalent technique to extend the hugely successful microrheology technique to study dynamical and mechanical phase transitions in nanoconfined soft complex materials at interface is highly desirable.

Video microscopy based particle tracking measurements have been used earlier mostly at the air-water interface [13,35–37] and recently at a fluid-fluid interface [38–40]. Most of these measurements as well as theoretical effort [41] have focused on extracting the viscous properties of the bare fluid-fluid interface and establishing conditions under which interface properties can be unambigously separated from bulk values. The experimental studies have mostly focused on purely viscous monolayers or freestanding soap films [38–40] including the work done in the group of Rondelez on monolayers of lipids to extract the surface concentration dependence of viscosity of these monolayers [14]. Recently,

the measurements have been also extended to a fluid-gel interface [42]. However, this measurement was not performed using controlled variation of surface concentration that is only possible with the LB method. Similarly, possibility of interface microrheology at air-fluid interface has been demonstrated using a method similar to that of Fuller's group but using much smaller diameter magnetic nanowire as a probe [43]. Here again, the focus is on establishing conditions of interface stress sensitivity and comparison of surface to bulk drag on the immersed probe. Recently, a scheme for performing interface microrheology (IMR) on Langmuir monolayers has been developed [44] based on ~ 1 μm beads trapped using optical tweezers. The technique is a step in the right direction and significantly enhances the measurable frequency range from 10 Hz to 10 KHz. However, the surface sensitivity would still be lower unless high viscosity monolayers are used. Moreover, it would be impossible to estimate the local viscoelastic modulus for heterogeneous monolayers. However, fluorescence based probe particle tracking methodology has not been used in any of these measurements. Here we have developed a new platform for controlled study of the dynamics of soft and granular materials in quasi-2D confinement by combining the two powerful and versatile techniques—LB and MR—using LB trough and fluorescence laser scanning confocal microscopy (FLSCM). Here we discuss results of IMR measurements on Langmuir monolayers of various soft materials including a standard surfactant, arachidic acid (AA), two nonglassy polymers polymethyl acrylate (PMA) and polyvinyl acetate (PVAc), and a glassy polymer polymethyl methacrylate (PMMA). All these monolayers, existing in the form of highly confined materials, were systematically compressed so that they undergo mechanical transitions and the IMR measurements were performed, *in situ*, at various surface densities. The resulting monolayers are expected to have varying degrees of viscoelasticity depending on surface concentration and, hence, offers the possibility of extracting the respective surface moduli. The frequency dependence of the extracted viscoelastic moduli for these different materials showed clear variations indicative of the differences in the mechanical properties as a function of respective surface densities. A significant advantage of our method is the extreme sensitivity to viscoelastic transitions occurring in low viscosity films due to the usage of a nanometer size quantum-dot (QD) probe [18,20]. In addition the small size of the probes allows extraction of spatially resolved viscoelastic properties of heterogeneous monolayers, as will be shown later.

II. EXPERIMENTAL DETAILS

Monodisperse cadmium selenide (CdSe) probe QDs capped with trioctylphosphine oxide (TOPO) were synthesized following the method of Peng *et al.* [45]. Synthesized CdSe QDs were cleaned several times using methanol followed by centrifuging to remove excess reagents and extract powders of CdSe. Diameter of the CdSe QDs were estimated to be around 9 nm from UV visible absorption spectroscopy and transmission electron microscope (TEM) measurements (Fig. 1). Solutions of CdSe particles of concentration

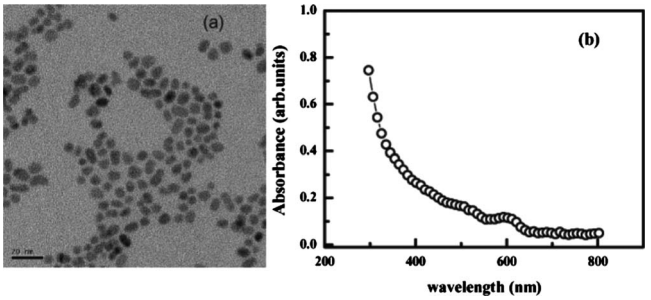

FIG. 1. (a) TEM image of the CdSe QD. The QDs appear to be fairly monodisperse with an estimated mean diameter of 9 nm. (b) UV-visible absorbance data for the QDs dispersed in chloroform. Formation of fairly monodisperse QDs is clearly evident from the existence of two exicitonic absorption peaks.

0.4 mg/ml were prepared using chloroform (Sigma Aldrich, 99.9%) and mixed with solutions of PMMA (Polyscience) of molecular weight (MW) 227 and 30 K, PVAc (Polymer Source) of MW 62 K, PMA (polymer source) of MW 172 K, AA (Sigma Aldrich), respectively. The concentration of the polymer solutions was 0.4 mg/ml. The ratio CdSe:PMMA, CdSe:PMA, CdSe:PVAc, and CdSe-AA in final solutions were optimized to avoid the effect of interparticle interaction on the dynamics of the probe particles. Final solutions, used for LB and IMR experiments, were stirred for 2 h before starting the experiment.

To prepare the Langmuir monolayers we used home-made Teflon trough of total area 142 cm^2 with temperature control and fitted with an fluorescence free optical quartz window (thickness=1 mm) at the bottom of the trough. This was used in combination with an LB instrument (KSV-Finland) with hydrophilic barriers made of Delrin. The entire trough was further enclosed in a air-tight optically transparent container to ensure thermal stability and minimize drift due to convection and temperature variations (Fig. 2). The trough and barriers were cleaned carefully with ethanol and deionized water (Barnstead, resistivity 18.2 MΩ/cm). Monolayers at the air-water interface were obtained by spreading solutions (35 μl) of the polymer and CdSe QD, using Hamilton microsyringe, onto the water surface of trough at room temperature (27 °C) and waiting for 20 min to let the spreading solvent evaporate. After evaporation of the solvent, lateral compression and expansion of the monolayer leads to reversible and hysteresis-free isotherms. Before each measurement two cycles of compression and decompression were performed to make the respective monolayers homogeneous. Surface pressures ($\Pi = \gamma - \gamma_0$) were determined using a Platinum Wilhelmy plate. Compression and decompression of the monolayers were performed at 10 mm/min. The LB trough was mounted on the inverted microscope stage (DMI 6000 CS) of a FLSCM from Leica, Germany (TCS SP5). We used a 50× objective (numerical aperture 0.5, free working distance=8.2 mm, *xy* resolution=390 nm) for imaging the QD embedded monolayers with variable exposure times. Argon (488 nm) laser were used for excitation and the emission (fluorescence) was observed in the 600–620 nm wavelength range. The fluorescence was separated from the excitation light by a dichroic beam splitter. The spectral resolution of

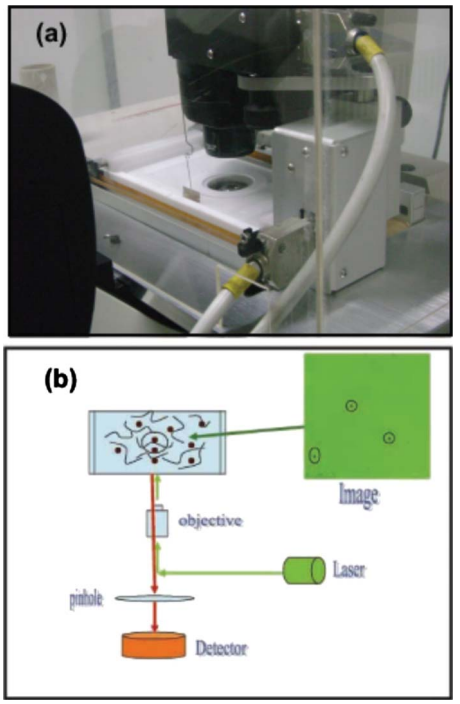

FIG. 2. (Color online) (a) Photograph of the experimental setup with the temperature controlled LB trough resting on the inverted microscope stage of a Leica LSCM. (b) Schematic of the experimental setup. A typical confocal image of a polymer monolayer surface with fluorescent QD probe particles is shown on the right.

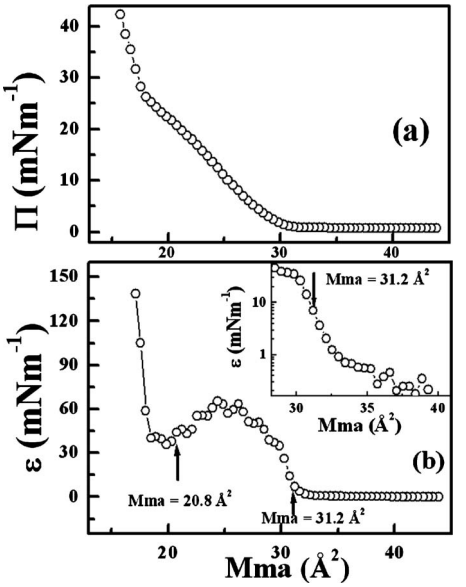

FIG. 3. (a) Surface pressure Π vs mean molecular area (Mma) isotherms of arachidic acid embedded with CdSe QD monolayers. (b) Isothermal compression modulus $\varepsilon = -A\frac{\partial \Pi}{\partial A}|_T$ for the same showing clearly the structural transitions in the monolayer, where A is the mean molecular area. The arrows indicate the respective Mma of the monolayers at which IMR measurements indicate viscoelastic transition. Inset: zoomed view of ε at higher Mma. The arrow indicates the Mma at which we observe a viscoelastic transition in IMR measurements.

the LSCM is 2 nm. The intensity of laser was adjusted continuously via an acousto-optical tunable filter (AOTF) while the reflected light was collected using a photomultiplier tube (PMT). Time series of confocal *XY* images of the QD embedded monolayers were collected by fixed trough areas (or Γ). The exposure times varied from 0.05 to 2 s with a pixel resolution from 50–500 nm depending on the number of pixels used. The typical QD probe density in the monolayer was $\sim 5 \times 10^{-4}$ μm^{-2}.

III. RESULTS AND DISCUSSIONS

A. Isotherms and compression modulus

Both our measurements and earlier data [46] indicate that the air-water interface is a bad interface for PMMA with a 2D Flory exponent $\nu \simeq 0.55$. Hence, the respective radius of gyration, $R_g = aN^{\nu}/\sqrt{6}$, of the PMMA polymers are 2.6 nm ($N=60$), 6.2 nm ($N=300$), 12 nm ($N=1000$), 19 nm ($N=2270$). Here a is the statistical segment length of PMMA. It is also known that for both PMA and PVAc, the air-water interface is a good solvent [46–48] and the 2D Flory exponent is $\nu \simeq 0.75$. Using this value one can estimate R_g for PMA 172 K ($N=2000$) to be 78 nm and that for PVAc 62 K ($N=1454$) to be 17 nm. To estimate the thickness of the monolayers, we transferred the monolayers at concentrations above Γ^{**} onto silicon substrates using a modified Langmuir-Schaefer method [47]. The respective thicknesses of the transferred monolayers of PMMA, PVAc, and PMA were estimated using ellipsometry (Sentech, Germany). It turns out that the thicknesses of the transferred monolayers varied between 2–3 nm for the various monolayers. In Fig. 3(a) we show a typical surface pressure, Π—area (Mma) isotherm of AA monolayers with CdSe QD embedded in it. The isotherm is typical of AA [10] monolayers, with clear evidence of a liquid-solid transition occurring between mean molecular area (Mma) of 30–18 Å^2. The isothermal compression modulus, ε, as shown in Fig. 3(b), also increases from Mma of ~30 Å^2 and goes through a maximum within the liquid-solid coexistence region followed by a decrease upto ~20 Å^2 after which there is a steep rise in the modulus indicative of formation of a solid and highly elastic monolayer. Similarly, the nature of typical isotherms for a glassy polymer, PMMA, of two different molecular weights, are shown in Figs. 4(a) and 4(b). The bulk glass transition temperatures, T_g, of these polymers are 120 °C (227 K) and 115 °C (30 K) [49], respectively. The respective compression moduli as a function of the surface concentration, Γ are shown in Figs. 4(c) and 4(d). Above a certain minimum concentration $\Gamma = \Gamma_{min}$ two crossovers in ε can be clearly observed. At $\Gamma = \Gamma^{**}$ the monolayer crosses over from semidilute to the concentrated region. An additional transition can be observed at Γ^{***}. Each of these transitions are also indicative of possible changes in viscoelastic and mechanical properties of the monolayers for which a surface rheological measurement is required. The isotherms for two nonglassy (under ambient conditions) polymers, PVAc ($T_g = 35$ °C) and PMA ($T_g = 15$ °C) are shown in Figs. 5(a) and 5(b), respectively. The respective compression moduli, shown in Figs. 5(c) and 5(d), indicate the main transitions at $\Gamma = \Gamma^{**}$.

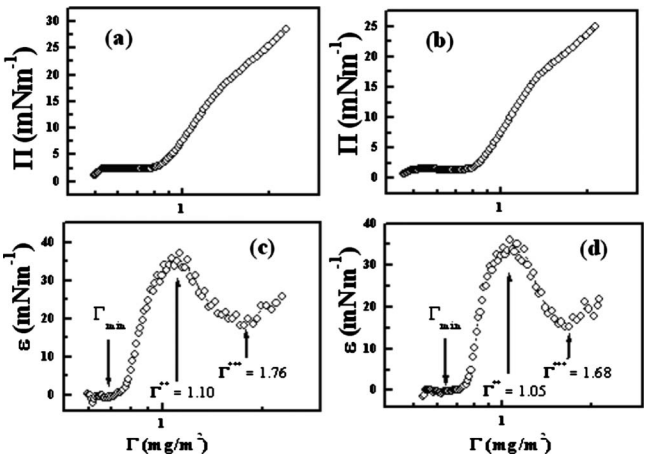

FIG. 4. Π-(Γ) isotherms of monolayers for (a) PMMA 227 K with CdSe QD (b) PMMA 30 K with CdSe QD. Isothermal compression modulus $\varepsilon = \Gamma \frac{\partial \Pi}{\partial \Gamma}|_T$ for (c) PMMA 227 K (d) PMMA 30 K. The respective crossover concentrations $\Gamma = \Gamma^{**}$, Γ^{***} are indicated by vertical arrows.

B. Interface microrheology

Here we describe details of the methodology of IMR measurements that were performed using the Langmuir trough and a LSCM on the systems that were described in the previous section. Interface microrheology data were collected at different points along the Π-Γ (or Π-area) isotherms at constant temperature (27 °C), as described earlier. In Fig. 6 we show typical embedded CdSe QD particle trajectories in respective media (refer caption for details). While comprehensive understanding of the particle dynamics and hence the underlying mechanical properties of the embedding medium can only be understood by detailed analysis of the nature of the mean-squared displacement (MSD) and the resulting micro-rheological moduli, the trajectories nevertheless, provide a preliminary idea about the mechanical properties of

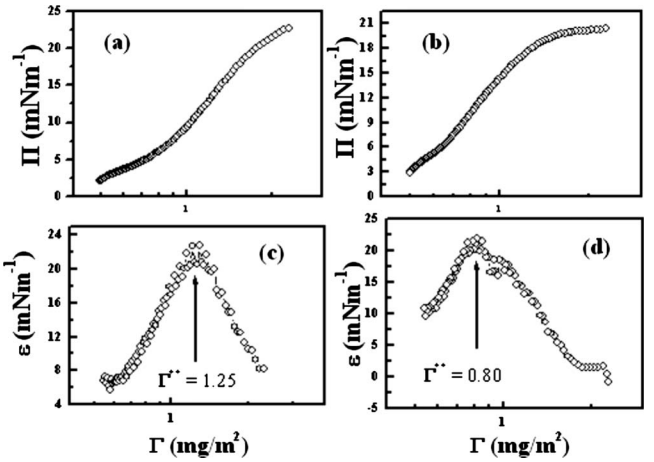

FIG. 5. Π-(Γ) isotherms of monolayers for (a) PVAc 62 K (b) PMA 172 K with embedded CdSe QD. Isothermal compression modulus ε for (c) PVAc 62 K (d) PMA 172 K. The arrows indicate respective concentrations $\Gamma = \Gamma^{**}$ for crossover of the monolayers from semidilute to concentrated region.

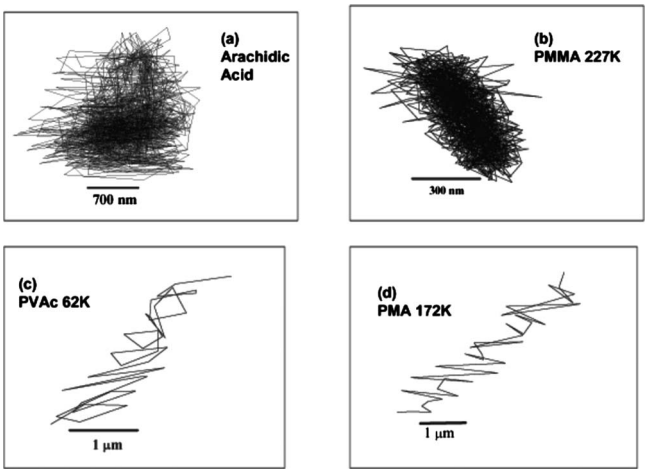

FIG. 6. Typical 2D trajectory of a QD probe particle in monolayers for (a) arachidic acid at Mma=23.4 Å^2 (b) PMMA 227 K at $\Gamma = 1.40$ mg/m^2 (c) PVAC 62 K at $\Gamma = 1.55$ mg/m^2 and (d) PMA 172 K at $\Gamma = 1.55$ mg/m^2. The scale bars are indicated in the respective panels.

the medium. For example, the particle trajectories in PVAc and PMA are indicative of simple diffusive behavior and hence the indicative of an underlying, predominantly, viscous medium. On the other hand the trajectories in PMMA and AA are indicative of fluid medium with significant elasticity.

Mean-square displacements were calculated by calculating the positions of the particles in the image using Image-J software. The motion of the particles in monolayers at water/air interface consisted of random diffusive motion and convective drift induced by the convection of air above the surface. The convective drift velocity was determined by the ensemble average over the velocities of the individual particles as well as over the respective imaged frames, using equation [50]

$$v(t) = \frac{1}{N}\sum_{i=1}^{N}\left\langle \frac{x_i(\tau+t) - x_i(\tau)}{t} \right\rangle, \tag{1}$$

where t is the lag time and $\langle .. \rangle$ denotes the average over the number of pairs of imaged frames (typically ~100–1000), for a given lag time t, and N is the number of particles per frame, which is typically around 4–5. Then diffusive particle motion was computed by calculating the displacement of the particle with mean drift of all particles being subtracted using equation

$$\Delta x(t,\tau) = x(\tau+t) - x(\tau) - \int_t^{\tau+t} v(\tau')d\tau', \tag{2}$$

The MSD of single particle was calculated from time average using

$$\langle \Delta x^2(t) \rangle = \frac{1}{T-t}\int_0^{T-t} \Delta x^2(t,\tau)d\tau, \tag{3}$$

For particles moving at a fluid interface the MSD, $\langle \Delta x^2(t) \rangle$, can be defined as $4D_{2D}t$ where D_{2D} is the 2D dif-

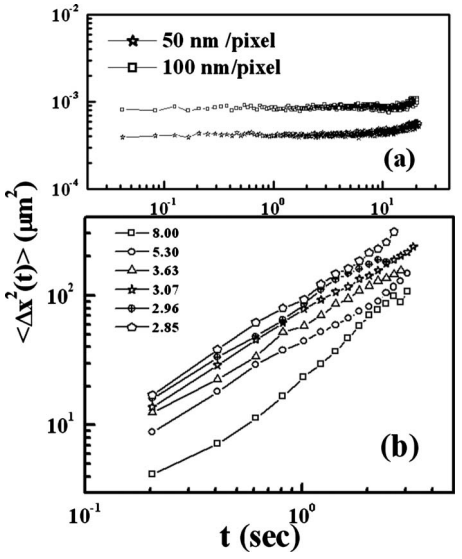

FIG. 7. MSD of tracked QD probe particles. (a) Probes spin coated with polymer on glass slides at room temperature and (b) freely diffusing on the surface of water. The numbers in (a) indicates the spatial resolution of the imaged frames in the respective data. All the image frames were collected with the resolution of 50 nm/pixel. The density Γ at which measurements on monolayer of CdSe QD were performed are indicated in the panel in mg/m^2 in (b).

fusion coefficient and takes the form derived by Saffman and Delbruck as [51],

$$D_{2D} = \frac{K_B T}{4\pi\eta_s}\left[\ln\left(\frac{\eta_s}{\eta R}\right) - \gamma_E\right], \tag{4}$$

where K_B is the Boltzmann constant, T the temperature, η_s is surface viscosity of a monolayer on water, η is the bulk viscosity of water, γ_E is the Euler's constant (=0.5772) and R is the radius of the probe particles. We further provide estimates of the resolution of the technique in terms of the smallest MSD that can be measured. In Fig. 7(a) the calculated MSDs for our QDs spin coated on a glass slide in a PMMA matrix at room temperature, for two different imaged pixel sizes, is shown. Since at room temperature the QDs are expected to be static in the PMMA matrix, this provides an estimate of the spatial resolution dependent static error in MSD inherent to the technique. As will become evident later, for all the data presented here the MSD values are higher that this minimum value and hence are not affected by resolution limited noise, as observed earlier [38]. In order to verify that the conditions at the air-water interface were similar to earlier video microscopy based particle tracking measurements we calculated the MSD for bare CdSe particles on water at various surface concentrations as shown in Fig. 7(b). Using the concentration dependent diffusion data we could verify the surface concentrations of CdSe for which interparticle interactions significantly affect the observed motion of individual particles.

To quantify the surface sensitivity of our method we provide below estimates of the Boussinesq number, $B_0 = \eta_s / \eta R$, for some of typical monolayers. As is well known, the Boussinesq number, B_0 is a crucial parameter, which determines the sensitivity of an interfacial rheology device to interface mechanical and rheological properties, in general, and stress in particular [52,53]. A high value of $B_0 (B_0 \gg 1)$ implies strong sensitivity to the interface rheological properties while a low value $(B_0 \ll 1)$ indicates reduced sensitivity to surface stresses. To estimate B_0 for our monolayers and hence to obtain an idea about the sensitivity of our measurements to surface rheological properties we have used both literature values for surface shear viscosities as well as estimates from our own measurements. Using the viscosity of water at 27 °C as 1.24×10^{-3} Pa s, radius of QD probe particles, R, as 5 nm and surface viscosity estimates for phospholid monolayers [13,14] $\eta_S \sim 10^{-10}$ Ns/m, $B_0 \sim 20$. Similarly using the MSD data for our PMA monolayers, which are viscous over the entire range of surface concentrations and Eq. (4), η_S can be estimated to be $\sim 10^{-8}$ Ns/m. Using the above estimate from our monolayers it turns out that $B_0 \sim 2000$. Clearly, our measurements are very surface sensitive and hence the above estimates for the shear modulus can indeed be taken to represent intrinsic properties of the monolayers. The enhanced sensitivity, obviously comes from the significantly smaller size of the probe particles used as compared to other measurements of interface rheology [13,18,20,44,53]. In addition we have also looked at the surface sensitivity in terms of the Saffman-Delbruck, l_0 defined as $l_0 = \eta_S / \eta$ [54,55]. Using the values of η_S and η as discussed above we find l_0 to be ~ 13 μm. Using the value of radius of our QD probe particles as 4.5×10^{-3} μm, we find that $R/l_0 \ll 1$ implying that the drag experienced by our probe particles in the respective monolayers are essentially 2D in nature.

This high-surface sensitivity allows determination of subtle viscoelastic transitions occurring in monolayers with low modulus, which would otherwise be difficult to observe with interface rheology [18,19] or the recently developed interface microrheology methods based on optical tweezers with ~ 1 μm beads or with magnetic nanowires.

Having established the appropriate conditions suitable for IMR we performed several measurements on monolayers with widely different characteristic. Figure 8 shows MSD for probe motion in AA at various mean molecular area. Clear trends in the change of the nature of the MSD with increasing area is observable. Most notably, at the lowest molecular area we find that the MSD has a strong plateau—it is almost independent of time—indicative of probe particle motion in a highly elastic medium. At the highest surface Mma, the motion of the QD, on the other hand, is almost diffusive indicative of a more viscous liquidlike condition of the embedding medium. It might be noted that the lowest area corresponds to the point where both the pressure and the compression modulus starts rising steeply [refer Fig. 3(b)]. This point is well known from structural studies on arachidic and other related fatty acids as the onset of the solid ordered phase [56]. Similarly, at the highest measured area there is a transition of the monolayer from the gaseous to the liquid or liquid condensed phase [56]. The viscoelastic nature of the underlying phases will become clear from evaluation of the respective interface microrheology parameters. We have also analyzed MSD data for different embedded probe QDs from

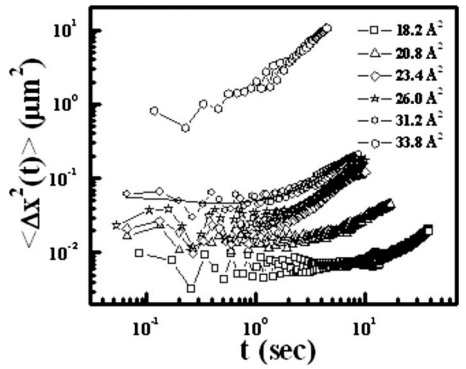

FIG. 8. MSD of QD probe particles embedded in arachidic acid monolayers. The Mma at which measurements were performed are indicated in the respective panels. The solid line indicates the power law profile, similar to Eq. (7), used to represent the MSD in Eqs. (5) and (6) to obtain the corresponding viscoelastic moduli

the arachidic acid monolayer at the same Mma in order to observe possible spatial dependence of the viscoelastic properties of the monolayer. In Fig. 9, we show MSD for three typical particles at two different Mma of arachidic acid within the liquid-solid co-existence region. It is known that within this region the morphology of the monolayers are quite heterogeneous with the random distribution of solid and liquidlike domains. It is quite likely that if one is able to track the motion of a large number of embedded QDs, which are randomly distributed in the monolayers, it would be possible to detect differences in the respective MSDs depending on whether the probes are embedded in a solidlike or fluidlike domain. Quite interestingly we find, especially for lower Mma [Fig. 9(a)], that the tracked particle shows subtle differences in MSD. Although, it is not possible to image or specify the location of the probes in domains having differ-

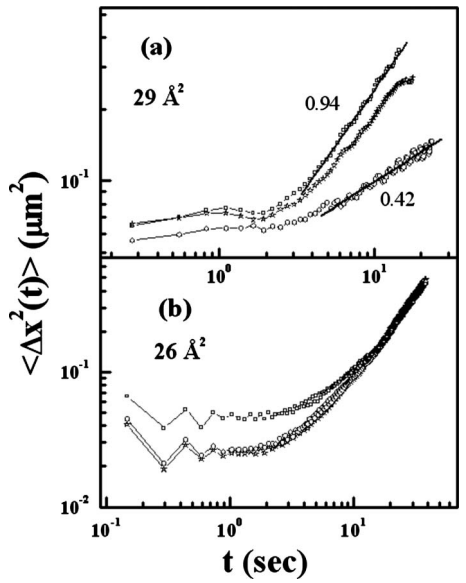

FIG. 9. Variation of MSD for different probe particles at Mma of (a) 29 Å^2 and (b) 26 Å^2 for arachidic acid monolayer. The slopes of the long time variation of MSD is indicated alongside the respective data.

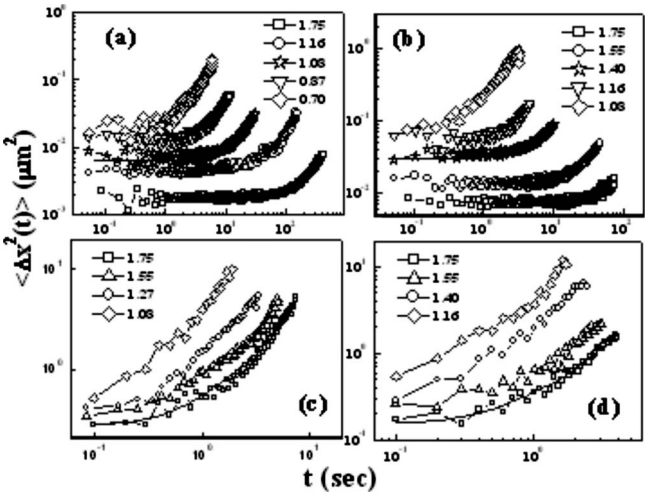

FIG. 10. MSD for monolayers with embedded QD for (a) PMMA 227 K, (b) PMMA 30 K, (c) PVAc 62 K, and (d) PMA 172 K. The density Γ at which measurements were performed are indicated in the respective panels in mg/m^2. The solid lines in the respective panels indicates the power law profile, similar to Eq. (7), used to represent the MSD in Eqs. (5) and (6) to obtain the corresponding viscoelastic moduli

ent ordering, this is a likely reason behind the observed difference in the MSDs. Differences are also observed for the MSDs collected on probe particles at lower Mma [Fig. 9(b)] although the MSDs are qualitatively much more similar to each other than those in Fig. 9(a). This could be expected since with increasing compression, more and more solidlike domains nucleate in the monolayer and hence chances of observing significant differences in viscoelastic properties among domains decrease considerably as the liquid-solid transition point is approached. It might be noted that such heterogeneity was observed in recent multiparticle tracking microrheology measurements, using large colloidal beads, in adsorbed protein layers at the air-water interface [57].

We next studied the IMR for various polymeric monolayers having widely different chemical as well as physical properties such as glass transition temperature etc. Figure 10 shows the respective MSD as a function of time, τ, for all the above polymers. Once again strong differences between the nature if MSD for the different polymers are observed. While the MSD for PMMA 227 K and PMMA 30 K show clear onset of a plateau at short and intermediate time followed by a long time diffusive regime at high surface concentrations, Γ, that for PVAc 62 K and PMA 172 K indicate diffusive or mildly subdiffusive nature of probe particle displacements over the entire observation time scale, even at the highest surface concentrations.

To obtain better insight into the viscoelastic transitions underlying the observed variations of MSD with nature of polymer or surface concentration we decided to extend the well developed formalism of extraction of microrheological parameters of bulk materials, from MSD of probe particles, to the interface. We describe in the following the methodology adopted to extract the IMR parameters from the observed interface probe particle displacements of materials existing in a highly confined state in the form of monolayers at the air-water interface.

The linear viscoelastic moduli $G_{2D}(s)$ for an 2D isotropic medium can be estimated following equation such as [28,58]

$$\widetilde{G_{2D}}(s) = \frac{2K_BT}{3\pi s\langle \Delta \tilde{x}^2(s)\rangle}, \tag{5}$$

To evaluate $G_{2D}(s)$ we have to calculate $\langle \Delta x^2(s)\rangle$ from $\langle \Delta x^2(t)\rangle$, the MSD in time domain by using numerical Laplace transformation using the following relation [58]

$$\langle \Delta x^2(s)\rangle = \int_0^\infty \langle \Delta x^2(t)\rangle e^{-st} dt. \tag{6}$$

For performing this transformation we have as assumed that the MSD is an explicit function of time which we have modeled as

$$\langle \Delta x^2(t)\rangle = at^\alpha + bt^\beta, \tag{7}$$

where the α represents the slope of the short time and β the long time part of MSD. We found that $0.03<\alpha<0.09$ and $0.4<\beta<1.0$ in the obtained data. To obtain the frequency dependent modulus we put in Eq. (3) [58] $s=i\omega$, where ω is the frequency and identify $G^*_{2D}(\omega)$ as,

$$\widetilde{G^*_{2D}}(\omega) = \frac{2K_BT}{3\pi i\omega\langle \Delta \tilde{x}^2(i\omega)\rangle}. \tag{8}$$

The real and imaginary part of the resulting complex viscoelastic modulus $[G'_{2D}(\omega)]$, $G''_{2D}(\omega)$ can then be identified with the storage and loss moduli, respectively. Using this scheme we demonstrate the nature and variation of obtained interface viscoelastic moduli for the various systems described earlier. In our set up, currently we can cover a frequency range of 0.01–20 Hz, which is a significant improvement over what can be achieved using ISR. The high-frequency limit can be enhanced with faster confocal scanning. We would also like to highlight the work of Helfer *et al.* [59–61], which provides experimental and theoretical evidence of probe size dependent sensitivity of frequency dependence of surface power spectral density of micron-sized beads in optical traps in active microrheology measurements on fluid membranes. Specifically, it is clearly shown that there exists a cutoff frequency above which the rheological nature of a membrane, as probed by a bead, is determined by the viscous forces on it due to the surrounding fluid and is hence always diffusive while below it the viscoelastic nature of the membrane is probed. It turns out that the cutoff frequency depends on the elastic modulus of the membrane and is inversely proportional to the size of the bead. Helfer *et al.* have provided an estimate for this frequency for a typical bead size of 1 μm and a 2D elastic modulus of $\sim$1 μN/m of $\sim$200 Hz. However, if the bead size is increased to $\sim$200–300 μm then the cutoff frequency comes down to $\sim$1 Hz or less. This therefore restricts the possibility of observing viscoelastic transitions for typical ISR setups to monolayers having an 2D elastic modulus of $\sim$10 mN m, which would typically occur for very solidlike monolayers. On the other hand in our case, this cutoff frequency is expected to be $\sim$100 KHz or alternatively allows observation of viscoelastic transitions of low-2D elastic moduli systems of $\sim$1 nN/m within our measured range.

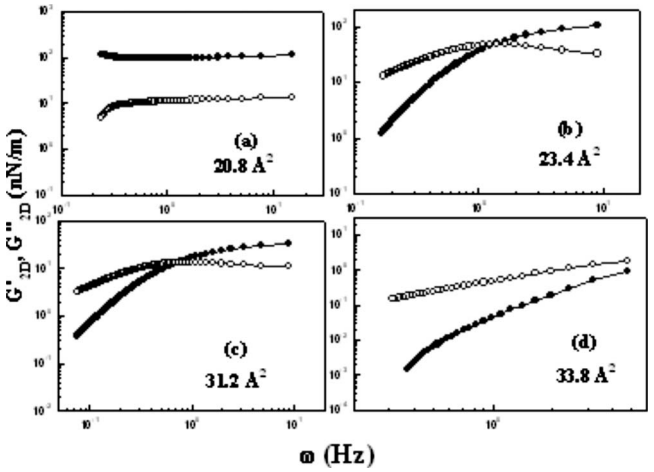

FIG. 11. Storage (G'_{2D}) (solid symbol) and loss (G''_{2D}) (open symbol) modulus for arachidic acid. Corresponding Mma are indicated in the respective panels. Evidence of viscoelastic transitions in the monolayer are clearly visible.

In Fig. 11 the obtained interface microrheological moduli for arachidic acid monolayer as a function of mean molecular area is depicted. The obtained viscoelastic moduli of the monolayer show two clear crossover from viscous liquid at Mma of 33 Å^2 ($G''_{2D}>G'_{2D}$) to a viscoelastic fluid at 31.8 Å^2 and further to a highly elastic solid at 20.8 Å^2 ($G'_{2D}>G''_{2D}$). The transitions also match well with the observed phase transitions as can be observed from the Π-area isotherms as well as from the isothermal compression modulus. Interestingly, we do not observe any transition across the area where the compression modulus goes through a maximum (Mma $\sim$23 Å^2). To emphasize the nature of the transitions further we show the variation of the extracted moduli, G''_{2D} and G'_{2D}, as a function of Mma for AA monolayers, for two frequencies in Fig. 12. While the crossover from viscous liquid to solidlike surface rheological behavior is clearly evident for both frequencies, similar to other surface rheological measurements [62], the more subtle frequency dependent transitions from viscous to viscoelastic behavior, which occurs above a certain frequency is only evident from our enhanced surface sensitive IMR measurements.

We next turn our attention to the case of a high T_g polymer—PMMA. As evident from Fig. 13, the qualitative

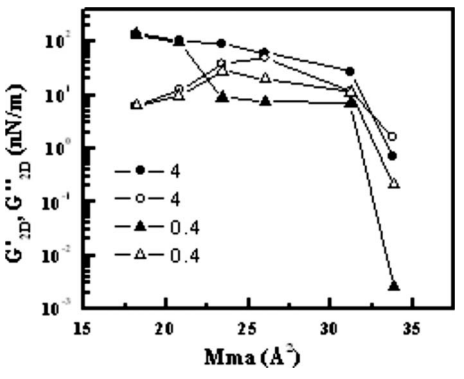

FIG. 12. G'_{2D} (solid symbol) and G''_{2D} (open symbol) vs Mma (Å^2) for Arachidic acid at two different frequencies (in Hz) indicated in the panels.

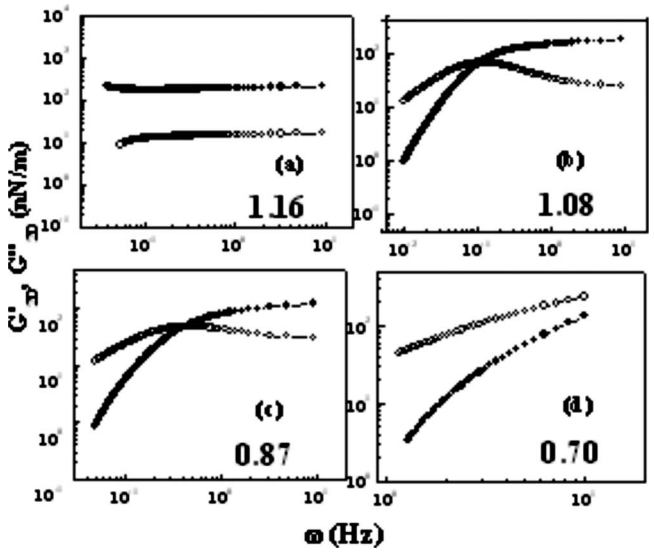

FIG. 13. G'_{2D} (solid symbol) and G''_{2D} (open symbol) for PMMA 227 K. The corresponding Γ values are indicated in the respective panels in mg/m^2.

nature is similar to that observed for AA. However, the transition from viscoelastic to elasticlike behavior is indicative 2D glass formation, as shown earlier [49]. Similar behavior is observed for the lower molecular weight (30 K) PMMA monolayer as indicated in Fig. 14. However, there are subtle differences in the obtained moduli between the low and high-molecular weight PMMA monolayers. For instance, the viscous-viscoelastic and the viscoelastic-elastic transitions occurs at higher surface concentrations, Γ, for the PMMA monolayer with higher molecular weight. The sensitivity of our technique to subtle variations in surface viscoelastic properties including onset of glassy behavior is thus well demonstrated.

Turning our attention to nonglassy (under ambient conditions) polymers we find similar sensitivity of the IMR technique to surface viscoelastic phase transitions. For monolayers of PVAc we find only one clear crossover point—the viscous-viscoelastic crossover at low Γ, as depicted in Fig. 15. However, upto the highest measured surface concentrations we do not find any other viscoelastic transitions, as was observed for PMMA or AA. We have not extended the measurements to higher concentrations since it is known that that the monolayers could buckle or collapse [47] and, hence, the observed behavior would not be representative of the monolayer. Finally, we have also studied a polymer which is chemically very similar to PMMA in order to establish whether the observed differences are related to the intrinsic viscoelastic condition of the polymer monolayers or are reflection of just the chemical interaction between the capped CdSe QD and the different polymers. It turns out that inspite of the chemical similarity of PMA to PMMA the viscoelastic nature of the PMA monolayers and their variation with surface density, as shown in Fig. 16, is closer to that of PVAc rather than PMMA. As mentioned earlier, the T_g of PMA is

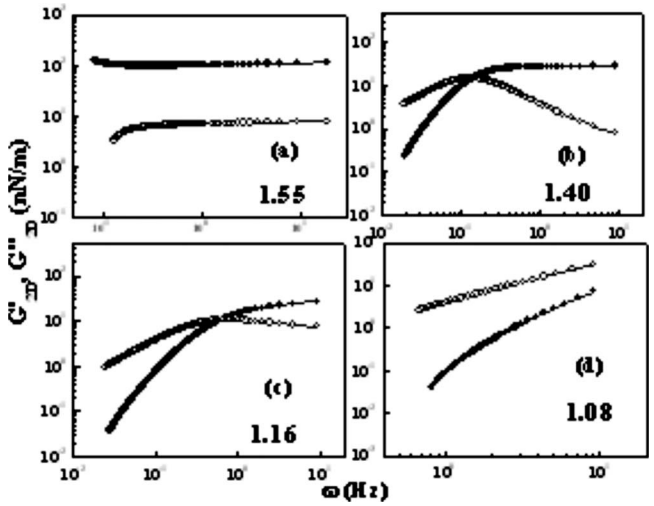

FIG. 14. G'_{2D} (solid symbol) and G''_{2D} (open symbol) for PMMA 30 K. The corresponding Γ values are indicated in the respective panels in mg/m^2.

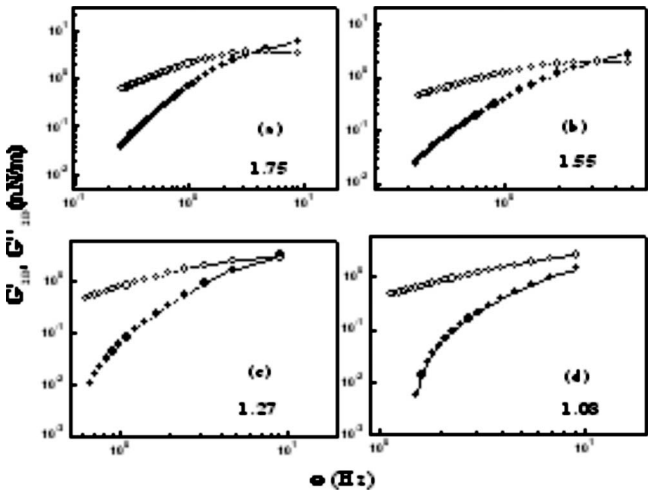

FIG. 15. G'_{2D} (solid symbol) and G''_{2D} (open symbol) for PVAc 62 K. The corresponding Γ values are indicated in the respective panels in mg/m^2.

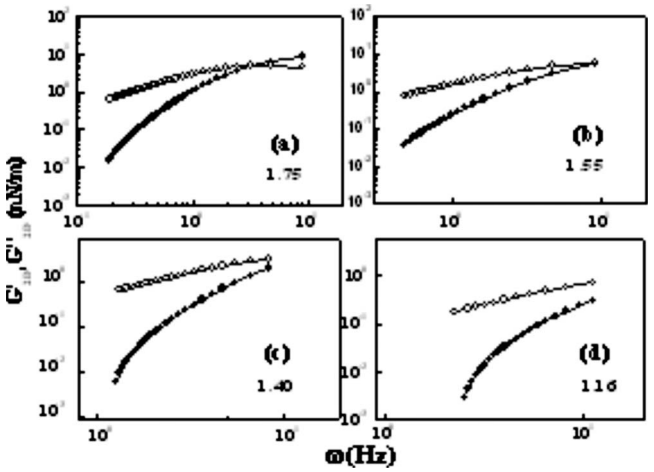

FIG. 16. G'_{2D} (solid symbol) and G''_{2D} (open symbol) for PMA 172 K. The corresponding Γ values are indicated in the respective panels in mg/m^2.

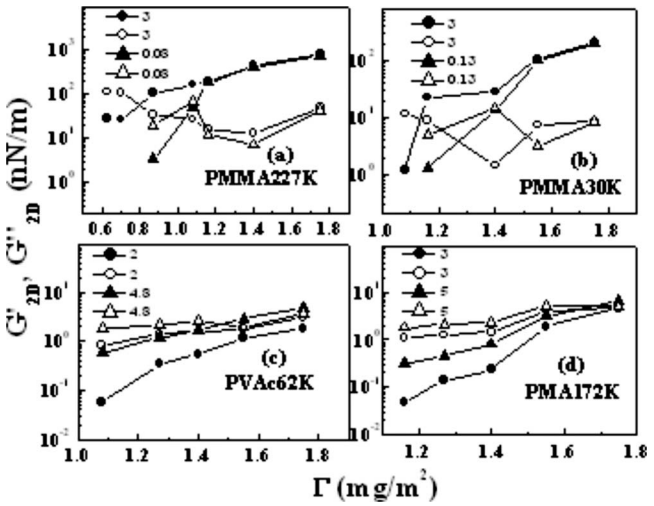

FIG. 17. G'_{2D} (solid symbol) and G''_{2D} (open symbol) vs surface density (mg/m^2) for (a) PMMA 227 K, (b) PMMA 30 K, (c) PVAc 62 K, and (d)PMA 172 K. The corresponding frequency values are indicated in the respective panels in Hz.

closer to PVAc than PMMA and hence the observed behavior can be explained in terms of the respective similarities or differences in T_g and not to chemical nature. In Fig. 17, we display these the various rheological transitions that the investigated glassy and nonglassy polymer monolayers undergo as a function of Γ and ω. While for PVAc and PMA most of the interface rheological measurements do not detect any transitions other than a constant increase in the surface viscosity with increased surface concentration, our sensitive measurements do sense a viscous to Maxwell type viscoelastic fluid with increased concentrations which also depends on frequency. For PMMA monolayers, on the other hand, the high-concentration phase shows solidlike behavior, with the onset concentration decreasing with increasing molecular weight. Although, rheology measurements alone cannot distinguish between a solid phase and a glassy phase, our earlier work on similar systems [49], using a different estimate and direct evidence for glass formation does confirm that the solidlike phase is indeed glassy. However, at lower concentrations, subtle viscoelastic transitions are also observed which is unlikely to be detected by surface rheological measurements with lower sensitivity.

IV. CONCLUSIONS

In conclusion, we have described the methodology of interface microrheology, an extension of the well established bulk microrheology technique to the interface. The technique combines the power of two well-established techniques of Langmuir-Blodgett and laser scanning confocal microscopy. We have demonstrated the efficacy and sensitivity of this technique to surface viscoelastic properties of diverse range of highly confined soft materials. We demonstrate how for well known materials such as arachidic acid with well defined structural phase transitions, the IMR method detects subtle transitions in viscoelastic properties which correspond quite closely to the structural phase transitions. Moreover, we provide evidence for subtle spatial variations in viscoelastic properties of the monolayers at fixed surface density by observing motions of multiple particles. Such variations are likely connected with the underlying structural heterogeneity, expected in such monolayers in the liquid-solid co-existence region and would be difficult to observe by other interface rheological or micro-rheological methods using much larger probes, as compared to what has been used here. Measurements on low and high-glass transition polymers also show the sensitivity of the technique to subtle variations in surface mechanical properties underlying dynamic transitions like the glass transition. We believe that this technique, with the demonstrated enhanced surface sensitivity, has the potential to unravel, through *in situ* measurements, subtle features in dynamical phase transitions with spatial resolution for diverse range of nanoconfined soft, glassy, and granular materials.

ACKNOWLEDGMENTS

A.K.K. and R.B. acknowledge CSIR for financial assistance.

[1] M. Alcoutlabi and M. McKenna, J. Phys.: Condens. Matter **17**, R461 (2005).
[2] Z. Fakhraai and J. A. Forrest, Science **319**, 600 (2008).
[3] R. D. Priestley *et al.*, Science **309**, 456 (2005).
[4] O. H. Seeck *et al.*, Europhys. Lett. **60**, 376 (2002).
[5] S. Srivastava and J. K. Basu, Phys. Rev. Lett. **98**, 165701 (2007).
[6] T. D. Li and E. Riedo, Phys. Rev. Lett. **100**, 106102 (2008).
[7] H. J. Wang *et al.*, Science **322**, 80 (2008).
[8] F. Bresme and M. Oettal, J. Phys.: Condens. Matter **19**, 413101 (2007).
[9] S. Srivastava *et al.*, J. Chem. Phys. **130**, 174718 (2009).
[10] A. Ulman, *An Introduction to Ultrathin Organic Films: From Langmuir-Blodgett to Self-Assembly* (Academic, London, 1991).
[11] F. Monroy, F. Ortega, R. G. Rubio, H. Ritacco, and D. Langevin, Phys. Rev. Lett. **95**, 056103 (2005).
[12] P. Cicuta, E. J. Stancik, and G. G. Fuller, Phys. Rev. Lett. **90**, 236101 (2003).
[13] M. Sickert, F. Rondelez, and H. A. Stone, EPL **79**, 66005 (2007).
[14] M. Sickert and F. Rondelez, Phys. Rev. Lett. **90**, 126104 (2003).
[15] L. Cristofolini, P. Cicuta, and M. P. Fontana, J. Phys.: Condens. Matter **15**, S1031 (2003).
[16] T. A. M. Ferenczi and P. Cicuta, J. Phys.: Condens. Matter **17**, S3445 (2005).
[17] G. T. Gavranovic, J. M. Deutsch, and G. G. Fuller, Macromol-

ecules **38**, 6672 (2005).
[18] C. F. Brooks *et al.*, Langmuir **15**, 2450 (1999).
[19] R. Krishnaswamy *et al.*, Langmuir **23**, 3084 (2007).
[20] T. A. Waigh, Rep. Prog. Phys. **68**, 685 (2005).
[21] A. S. Keys *et al.*, Nat. Phys. **3**, 260 (2007).
[22] J. Goyon *et al.*, Nature (London) **454**, 84 (2008).
[23] J. D. Ferry, *Viscoelastic Properties of Polymers* (Wiley, New York, 1980).
[24] R. G. Larson, *The Structure and Rheology of Complex Fluids* (Oxford University Press, New York, 1999).
[25] P. Chaudhuri, L. Berthier, and W. Kob, Phys. Rev. Lett. **99**, 060604 (2007).
[26] W. Kob, C. Donati, S. J. Plimpton, P. H. Poole, and S. C. Glotzer, Phys. Rev. Lett. **79**, 2827 (1997).
[27] K. Stratford *et al.*, Science **309**, 2198 (2005).
[28] P. Cicuta and A. M. Donald, Soft Mater. **3**, 1449 (2007).
[29] E. R. Weeks *et al.*, Science **287**, 627 (2000).
[30] W. K. Kegel and A. van Blaaderen, Science **287**, 290 (2000).
[31] D. T. Chen, E. R. Weeks, J. C. Crocker, M. F. Islam, R. Verma, J. Gruber, A. J. Levine, T. C. Lubensky, and A. G. Yodh, Phys. Rev. Lett. **90**, 108301 (2003).
[32] I. Y. Wong, M. L. Gardel, D. R. Reichman, E. R. Weeks, M. T. Valentine, A. R. Bausch, and D. A. Weitz, Phys. Rev. Lett. **92**, 178101 (2004).
[33] J. Sprakel, J. van der Gucht, M. A. Cohen Stuart, and N. A. M. Besseling, Phys. Rev. E **77**, 061502 (2008).
[34] J. Sprakel, J. van der Gucht, M. A. Cohen Stuart, and N. A. M. Besseling, Phys. Rev. Lett. **99**, 208301 (2007).
[35] J. Wu and L. L. Dai, Langmuir **23**, 4324 (2007).
[36] R. Zangi and S. A. Rice, Phys. Rev. Lett. **92**, 035502 (2004).
[37] A. H. Marcus, J. Schofield, and S. A. Rice, Phys. Rev. E **60**, 5725 (1999).
[38] V. Prasad, S. A. Koehler, and E. R. Weeks, Phys. Rev. Lett. **97**, 176001 (2006).
[39] V. Prasad and E. R. Weeks, Phys. Rev. Lett. **102**, 178302 (2009).
[40] V. Prasad and E. R. Weeks, Phys. Rev. E **80**, 026309 (2009).
[41] H. A. Stone and A. Ajdari, J. Fluid Mech. **369**, 151 (2006).
[42] E. K. Hobbie, S. Lin-Gibson, and S. Kumar, Phys. Rev. Lett. **100**, 076001 (2008).
[43] A. Anguelouch, R. L. Leheny, and D. H. Reich, Appl. Phys. Lett. **89**, 111914 (2006).
[44] R. Walder, C. F. Schmidt, and M. Dennin, Rev. Sci. Instrum. **79**, 063905 (2008).
[45] Z. A. Peng and X. Peng, J. Am. Chem. Soc. **123**, 183 (2001).
[46] R. Vilanove, D. Poupinet, and F. Rondelez, Macromolecules **21**, 2880 (1988).
[47] S. Srivastava and J. K. Basu, Phys. Rev. E **79**, 041603 (2009).
[48] F. Monroy, H. M. Hilles, F. Ortega, and R. G. Rubio, Phys. Rev. Lett. **91**, 268302 (2003).
[49] A. K. Kandar, R. Bhattacharya, and J. K. Basu (unpublished).
[50] P. Dhar *et al.*, J. Phys. Chem. B **112**, 9565 (2008).
[51] P. G. Saffman and M. Delbruck, Proc. Natl. Acad. Sci. U.S.A. **72**, 3111 (1975).
[52] Th. M. Fischer, P. Dhar, and P. Heinig, J. Fluid Mech. **558**, 451 (2006).
[53] S. Reynaert *et al.*, J. Rheol. **52**, 261 (2008).
[54] M. L. Henle and A. J. Levine, Phys. Fluids **21**, 033106 (2009).
[55] P. G. Saffman, J. Fluid Mech. **73**, 593 (1976).
[56] V. M. Kaganer, H. Mohwald, and P. Dutta, Rev. Mod. Phys. **71**, 779 (1999).
[57] M. H. Lee *et al.*, Langmuir **26**, 2650 (2010).
[58] T. G. Mason, Rheol. Acta **39**, 371 (2000).
[59] A. J. Levine and F. C. MacKintosh, Phys. Rev. E **66**, 061606 (2002).
[60] E. Helfer, S. Harlepp, L. Bourdieu, J. Robert, F. C. MacKintosh, and D. Chatenay, Phys. Rev. E **63**, 021904 (2001).
[61] E. Helfer, S. Harlepp, L. Bourdieu, J. Robert, F. C. MacKintosh, and D. Chatenay, Phys. Rev. Lett. **87**, 088103 (2001).
[62] K. S. Yim, B. Rahaii, and G. G. Fuller, Langmuir **18**, 6597 (2002).